ACS Catalysis

Research Article

pubs.acs.org/acscatalysis

Density Functional Theory Comparison of Methanol Decomposition and Reverse Reactions on Metal Surfaces

Rodrigo García-Muelas, Qiang Li, and Núria López*

Institute of Chemical Research of Catalonia (ICIQ), Avgda. Països Catalans 16, 43007 Tarragona, Catalonia, Spain

Supporting Information

ABSTRACT: Methanol decomposition on metals has been subject of several theoretical studies, usually concentrating on a particular set of reactions in the main reaction path. In this work, we present an extensive study that considers all potential elementary steps for four close-packed surfaces including Cu, Ru, Pt, and Pd that shows the different behaviors and alternative routes through which the decomposition can take place by theoretical methods, including dispersion contributions. Decomposition follows different paths on these metals; while Cu would produce CH_2O, CO is the major product for the other metals. In addition, coverage effects might change the first step in Pt and Ru from methylenic to alcohol H activation. Alternatively the reaction network can be inspected for the formation of methanol from CO and hydrogen. Under these conditions, Cu generates CH_2O and only at very high H coverages is methanol likely to appear. On Pd, methanol formation and CHOH dissociation compete, thus leading to an inefficient process. A similar path takes place for Pt. For Ru the lateral paths leading to C−O breaking can occur at several points in the reaction network, never reaching CH_3OH. A compilation of the results with comparable computational setups presents a detailed database that can be added to the thermodynamics and kinetics for other reactions, such as methanation, with which they share a common list of reactions, or employed when analyzing larger alcohols such as those derived from biomass.

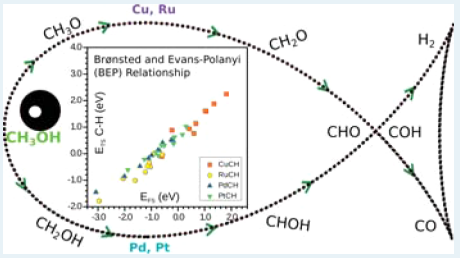

KEYWORDS: *methanol, density functional theory, Brønsted and Evans−Polanyi (BEP) relationships, Pt, Pd, Ru, Cu*

INTRODUCTION

Methanol is the smallest of all alcohols and, as it is a liquid and is easy to store, it has been presented as a potential energy vector that can be employed in new energy approaches. Indeed, the methanol economy concept was coined in the 1990s to account for this possibility.[1] The use of methanol in mobile applications seemed to be the most promising, as it can be directly used as fuel in combustion engines, directly converted to energy in electrochemical cells, or converted into another energy vector such as hydrogen.[2] Several of those approaches are based on its electrochemical transformation and the corresponding energy release, but the problem of direct methanol fuel cells comes from the strong adsorption of one of the subproducts, namely CO. Although methanol is currently produced by hydrogenation of a mixture of CO and CO_2 in a Cu/ZnO catalyst,[3,4] it is also possible to produce it from agricultural products and municipal waste, making it a recycled product. Methanol is also employed as a surrogate for larger biomass-derived alcohols,[5] even if this approach might be overly simple.

Methanol decomposition and synthesis on metal surfaces has been extensively investigated by several authors during the past decade. Greeley and Mavrikakis also investigated methanol decomposition on Cu(111),[6] where the preferred path would start by the dehydrogenation of the hydroxyl group. In the decomposition route on Pt(111),[7,8] the same authors studied a reaction network either starting with the dissociation of the alcohol hydrogen or starting from the methylenic H atoms. According to them, carbon dehydrogenation would be a preferred step, in contrast with the preferential O−H bond breaking found in experimental studies.[9] A recent study by the group of Campbell showed that the methoxy radical adsorbed on Pt(111) is rather unstable, as was predicted by DFT studies.[10] For the same system Neurock and co-workers[11] found that, under ultra-high vacuum conditions, methanol would desorb rather than react, as the activation barriers for the first dehydrogenation are higher than the desorption energy. In the study, two intermediates were discarded due to complexity, CHOH and COH; as we will show, both might belong to the minimum energy path. To rationalize the results for Pt, several attempts have been made. According to the d-band model, the activity of a metal is a function of the d-band center.[12−14] This analysis was employed by Park and co-workers[15] to study the methanol electrooxidation activity of Pt. In parallel, Ferrin and co-workers demonstrated that the catalyst performance for methanol electrooxidation can be described as a function of the free energy of adsorption of CO and OH radicals.[16] However, the adsorption energies and d-band positions are correlated, as the energies are a function of the d-band positions.[14] Yudanov and co-workers focused on C−O bond breaking on Pd nanoparticles, identifying it as a slow side process in the decomposition reaction.[17] On Pd and other metals, the

Received: November 3, 2014
Revised: December 23, 2014
Published: December 31, 2014

DOI: 10.1021/cs501698w
ACS Catal. 2015, 5, 1027−1036

decomposition or dehydrogenation steps have been compiled for a large range of molecules and fragments containing the same heteroatom.[18,19] As for Ru(0001), experiments have shown the coexistence of two paths, one leading to CO and the other one leading to C and O separate fragments, where the second path was identified as responsible for surface poisoning.[20] The reason is that H-assisted reactions have been found to lower the barriers to difficult decompositions such as that of CO.[21]

Completeness at any stage is thus crucial to understand intricate reaction networks that can be intercrossed. As the reaction set becomes quite large, there is a need to describe the fragments to generate a database that can be employed to predict the activation energies of each particular step. Furthermore, the database can be modified to include the particular cases of lateral interactions and/or solvents for a more adequate representation of complex electrocatalytic systems.

This is precisely the aim of the present work. For methanol, we have built a consistent complete reaction network that accounts for crossings between different paths at any time in a way similar to that which we reported for HCN synthesis.[22] The reactions considered in our network are presented in Scheme 1. For this set of reactions we have investigated the following items: (i) we have stablished a common connectivity matrix notation that allows extrapolation to more complex substrates; (ii) we have analyzed the role of different kinetic−thermodynamic relationships to ensure the best form to predict the energies for other metals; (iii) we have described the potential hysteresis in the decomposition/synthesis paths by inspecting the direct and reverse reactions; and (iv) we have analyzed lateral effects for key competitive routes.

Scheme 1. Reaction Network for the Decomposition of Methanol on the Different Surfaces Considered in This Work

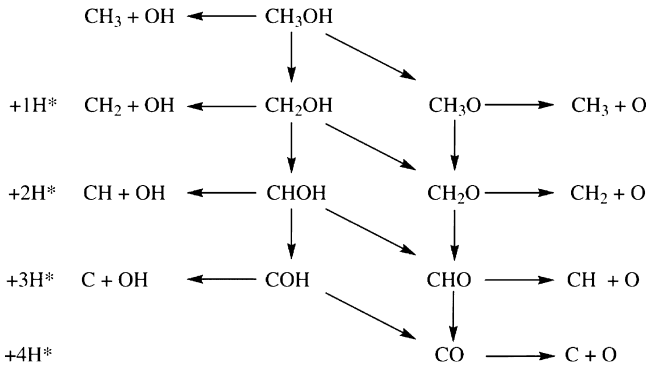

COMPUTATIONAL DETAILS

Slab calculations were performed using the Vienna ab initio simulation package (VASP),[23,24] the PBE density functional,[25] and a kinetic energy cutoff of 450 eV. The inner electrons were represented by projector augmented wave (PAW) pseudopotentials.[26,27] The calculated lattice parameters for Ru, Cu, Pd, and Pt are 2.712, 3.629, 3.939, and 3.968 Å, respectively, and $[c/a]_{Ru}$ = 1.581, in good agreement with experimental values of 2.706, 3.615, 3.893, and 3.924 Å and $[c/a]_{Ru}$ = 1.582.[28−31] The cells were built in a p (3 × 3) configuration for Ru and Cu, with a $2\sqrt{3} \times 2\sqrt{3} - R30°$ supercell. Therefore, the coverages are low and comparable, between 0.08 and 0.11 ML. To inspect lateral interactions in reaction and activation energies, we included one or two additional methanol molecules in the $2\sqrt{3} \times 2\sqrt{3} - R30°$ supercell. All metallic surfaces were modeled by a four-layer slab. The two topmost layers were fully relaxed, and the two bottom layers were fixed to the bulk distances. For surface calculations, the Brillouin zone was sampled by a Γ-centered *k*-point mesh generated through the Monkhorst−Pack method,[32] and the samplings were denser than 0.3 $Å^{-1}$. We included a vacuum region larger than 12 Å and a dipole correction along the *z* direction.[33] We also included the van der Waals (vdW) corrections by applying Grimme's DFT-D2 method,[34,35] with the C_6 parameters developed in our group.[36,37] The van der Waals contributions to adsorption can be found in Table S1 of the Supporting Information. The molecules in the gas phase were relaxed in a box of 20 × 20 × 20 $Å^3$. We employed both the nudged elastic band (CI-NEB) and the improved dimer method, (IDM) to find the transition states.[38−40] The optimization thresholds were 10^{-5} eV and 0.015 eV/Å for electronic and ionic relaxations, respectively. In all cases the saddle point nature of the transition states was assessed by the calculation of the numeric Hessian with a step of 0.02 Å and its diagonalization that rendered a unique imaginary frequency. In the following, all discussed energies correspond to dispersion-containing values including zero-point energy unless stated otherwise.

RESULTS

Description of the Reaction Network. The data for adsorption of key intermediates can be found in Table S1 in the Supporting Information. The contribution of van der Waals dispersion terms has been evaluated for reactants and products. Inclusion of vdW interactions raises (more exothermic) the adsorption values between 0.01 and 0.20 eV. Tests of different adsorption sites and comparison to previous results in the literature are provided in Tables S2−S4 in the Supporting Information. In order to simplify and order all of the intermediates, an identification vector that defines them has been developed (see Table S5 in the Supporting Information) which can be extended to more complex compounds. The vector defines the stoichiometry with the first three numbers (carbon, hydrogen, oxygen), and isomerism is given as a fourth number; thus, methanol corresponds to 1411 and CO to 1011.

In this section we describe all of the potential reaction steps described in Scheme 1 for all four metals in the present study: Cu(111), Ru(0001), Pt(111), and Pd(111). In Figures 1−3, we present top and side perspectives for all of the reaction steps in the paths for the particular case of copper. A complete version of these figures for all metals considered can be found in the final section of the Supporting Information.

The first group of reactions corresponds to the O−H bond breaking and contains four elementary steps starting from methanol (CH_3OH), hydroxymethyl (CH_2OH), hydroxymethylidene (CHOH), and hydroxymethylidyne (COH) (Figure 1). For adsorbed molecules, the initial configuration presents the OH fragment close to the surface and thus bond activation easily occurs. In the case of CH_2OH, both O and C atoms are bonded to the surface but the hydrogen on the OH group is closer to the surface in comparison to the methylenic H; thus, it seems rather straighforward that the OH is more activated at this stage. On the other hand, the CHOH and COH fragments are bonded to the surface by the carbon center (Figure 1), and thus the alcoholic hydrogens are farther away from the surface. Such kinds of configurations would be better activated by

DOI: 10.1021/cs501698w
ACS Catal. 2015, 5, 1027−1036

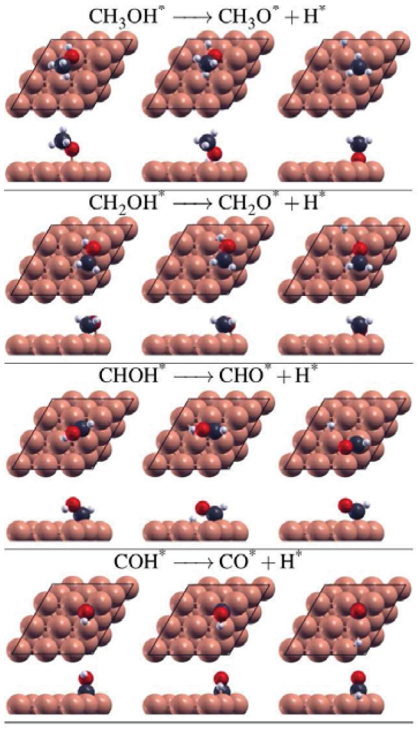

Figure 1. Schematic representation of the reaction steps considered for the decomposition on Cu(111), regarding O−H bond breaking. Large spheres correspond to metal atoms and red, gray, and white spheres to O, C, and H, respectively.

nearby structural defects on the metal surface.[41] Indeed, coordinative unsaturated atoms, such as those present on step sites, could be more effective to catalyze the perpendicularly adsorbed fragments, as they not only are more reactive but also prevent the rotation needed to activate the O−H fragment. In the final positions of methanol and COH decomposition the fragments stand up perpedicular to the surface. In comparison, the fragments with partially dehydrogenated C moieties (CH_2OH and CHOH) either lie on the surface or are just bonded through the C atom. For CH_3OH and CH_2OH, O−H activation implies a change in the coordination of the O atoms from top to fcc sites, Pt being the only exception. For CHOH or COH dehydrogenation, C moves from the bridge to the top site or keeps the fcc site, respectively.

Figure 2 illustrates the dehydrogenation of the carbon atom in six different molecules: CH_3OH, CH_3O, CH_2OH, CH_2O, CHOH, and formyl (CHO). In all cases a change in the coordination of the carbon atom to fulfill the empty valence is found.[42] In some cases, such as the dehydrogenation of CH_2OH, this is accompanied by a reorientation of the final carbon fragment CHOH which leads to O atoms no longer adsorbed to the surface. The rotation is induced by the larger empty valence of C atoms in comparison to O atoms.

The eight elementary steps for the C−O bond breaking are presented in Figure 3, corresponding to CH_3OH, CH_3O, CH_2OH, CH_2O, CHOH, CHO, COH, and CO. It is well-known that the CO decomposition is much easier at steps due to the stand-up nature of the adsorbed CO molecules and the fact that step atoms are more reactive; however, the rest can be analyzed for planar surfaces with a sufficiently high confidence. As we will see later, the obtained barriers are low enough to ensure that the remaining reactions can occur under mild experimental conditions.

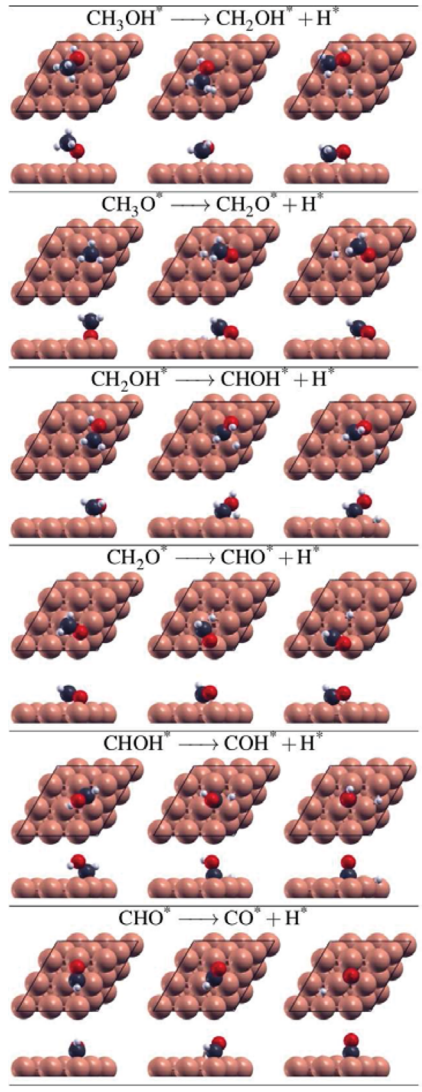

Figure 2. Schematic representation of the reaction steps considered for the decomposition on Cu(111), regarding C−H bond breaking. Large spheres correspond to metal atoms and red, gray, and white spheres to O, C, and H, respectively.

Energy Profiles for Dehydrogenation. The lowest energy paths for methanol decomposition on the different surfaces are shown in Figure 4. Reaction and activation energies are given in Tables S6 and S7 in the Supporting Information, and the structures are depicted in Table S13 in the Supporting Information. On Cu(111), the methanol decomposition pathway follows as $CH_3OH \rightarrow CH_3O \rightarrow CH_2O \rightarrow CHO \rightarrow CO + H_2$. It is the simplest pathway among all of the metals and is also supported by previous theoretical studies.[6,43−45] The first step consists of O−H bond breaking, which is slightly exothermic (−0.22 eV). However, this step presents a rather large energy barrier of 0.98 eV, which is 0.61 eV higher than the desorption energy. CH_3O is acknowledged as the most stable intermediate among all of the species during the decomposition process on Cu(111).[6,44−46] From CH_3O on, all subsequent reactions correspond to C−H breaking. The bond lengths of C−H in sequential TS structures are 1.86, 1.57, and 1.14 Å, respectively, which demonstrates that the C−H bond breaking occurs more easily with further dehydrogenations. In correspondence, the activation energy barriers are 1.04, 0.55,

DOI: 10.1021/cs501698w
ACS Catal. 2015, 5, 1027−1036

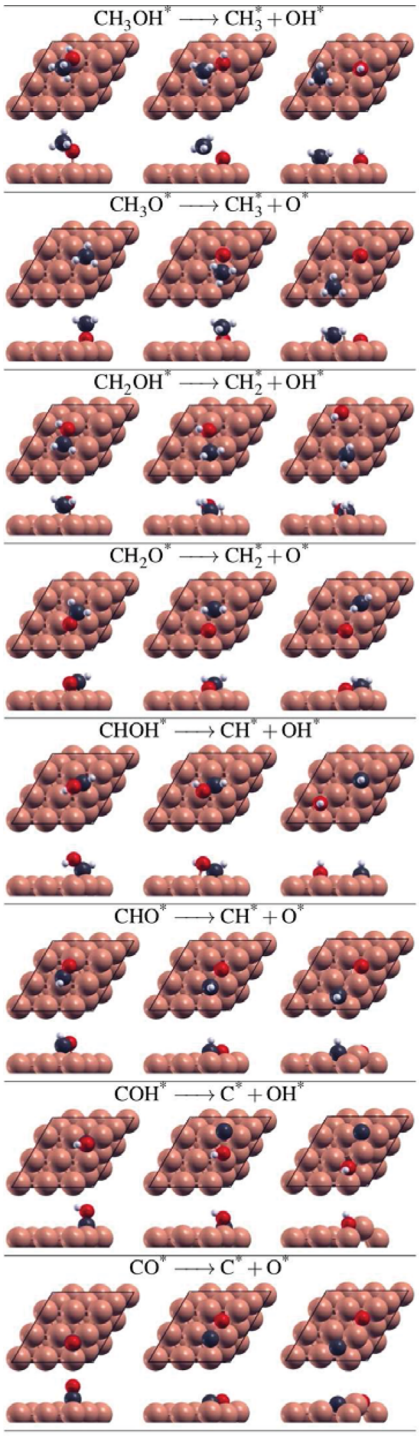

Figure 3. Schematic representation of the reaction steps considered for the decomposition on Cu(111), regarding C−O bond breaking. Large spheres correspond to metal atoms and red, gray, and white spheres to O, C, and H, respectively.

and 0.19 eV. Considering the required energy for O−H scission (0.98 eV), the dehydrogenation from CH_3O to CH_2O, which is also highly endothermic by 0.73 eV, is the most energy-demanding step in the decomposition pathway. The reported reaction (activation) energies for this step in previous theoretical studies are 0.97 (1.42),[6] 0.92 (1.27),[45] 0.85 (1.85),[44] and 1.00 (1.16)[43] eV, respectively. To enhance decomposition, any basic center on the carrier could thus be more adequate than the metal surface itself. Moreover, CH_2O can easily desorb from Cu(111) because its binding energy of 0.31 eV is less than the energy barrier for the dehydrogenation, 0.55 eV. When dehydrogenation continues from formaldehyde, then the C−H bond breaks directly or spontaneously from CHO with a lower energy barrier (0.19 eV) and a highly exothermic path (−0.99 eV). Similar results were obtained by Lim[43] (−0.89 eV) and Zuo[44] (−0.93 eV).

C−O bond breaking could only occur for the CHOH intermediate, but in the direct methanol decomposition path this intermediate is never observed. It has been suggested that in the presence of water the reaction network could continue through the condensation of CH_2O with an adsorbed OH and further oxidation to CO_2.[46]

On Ru(0001) surfaces, there are two competing pathways for methanol decomposition: on one side, $CH_3OH \rightarrow CH_3O \rightarrow CH_2O \rightarrow CHO \rightarrow CO + H_2$, and on the other, $CH_3OH \rightarrow CH_2OH \rightarrow CHOH \rightarrow COH \rightarrow CO + H_2$. The first path is the same as that on Cu(111); the O−H bond breaks first, and then the reaction proceeds for the C−H bonds. However, in the alternative pathway only C−H bond breaking occurs and the O−H bond is retained during the whole process until the final step, which leads to CO and H_2. Starting from methanol, both O−H and C−H bond breakages are exothermic with reaction energies of −0.74 and −0.39 eV and the required bond-breaking energies are 0.60 and 0.48 eV, respectively. Thus, C−H bond splitting is more kinetically preferable, while the O−H bond breaking which leads to the CH_3O is more favored thermodynamically. However, on the basis of experimental studies,[47] only methoxy species were observed in the temperature range from 180 to 340 K. In the first pathway, the dehydrogenation of methoxy to formaldehyde is the step with the highest energy demand, with an energy barrier of 0.90 eV. Unlike the formaldehyde desorption on Cu(111), formaldehyde binds strongly on Ru(0001) with a desorption energy of 1.09 eV, in good agreement with the study by Chiu (1.06 eV).[48] Moreover, the dehydrogenation from CH_2O to CHO occurs easily through a negligible barrier of 0.06 eV. The dehydrogenation of CHO is also almost barrierless (0.04 eV) and is highly exothermic (−0.90 eV). Our results are in good agreement with recent experiments for high methanol coverages, which report that O−H bonds break to form methoxy, which subsequently evolves to CO and hydrogen with no significant C−O bond breaking.[47] In the next section, we will analyze the effect of spectator methanol molecules for the first dehydrogenation reactions on Ru(0001) and Pt(111). Significatively, along the $CH_3OH \rightarrow CH_2OH \rightarrow CHOH \rightarrow COH \rightarrow CO + H_2$ path the three barriers are quite low, although two intermediates are higher in energy than those of the methoxy path. From a thermodynamic perspective, the elementary steps are not as favored as the first path and the first two reactions are only weakly exothermic: −0.39 and −0.43 eV, respectively. Moreover, the last H abstraction from COH to CO, although being exothermic (−0.76 eV), is hindered by a sizable energy barrier of 0.77 eV.

Carbon monoxide binds strongly on Ru(0001), Pd(111), and Pt(111) surfaces, with desorption energies of +1.93, +2.29, and +1.95 eV, respectively. At high methanol pressures, the reaction will proceed until all of these surfaces become covered by carbon monoxide, and further reactions will take place only after carbon monoxide desorbs. This is one of the most common problems for the direct methanol fuel cells that are usually described for Pt. In turn, methanol adsorption on such

DOI: 10.1021/cs501698w
ACS Catal. 2015, 5, 1027−1036

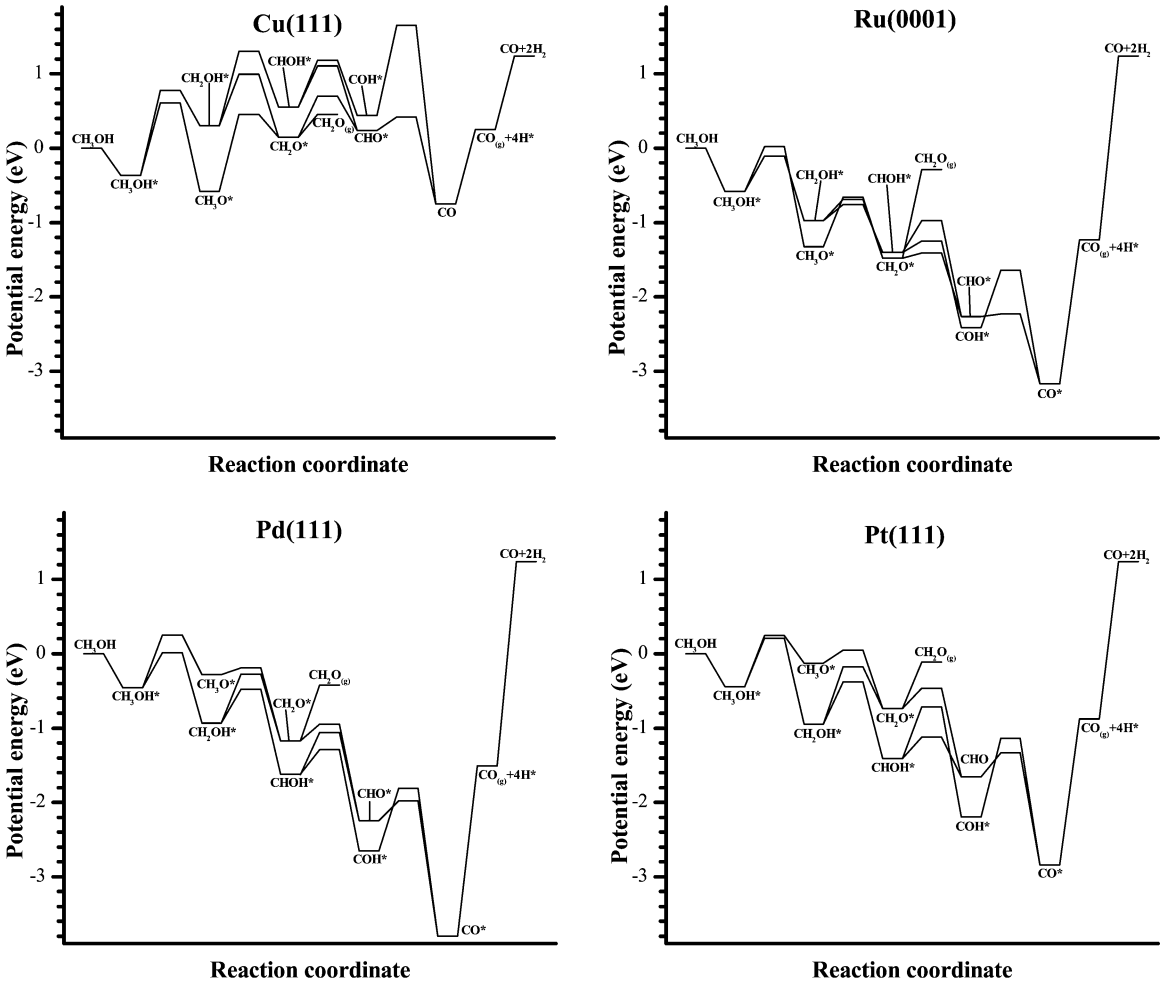

Figure 4. Reaction profiles for the decomposition of methanol to CO and H_2 on different metal surfaces. The minimum energy paths are considered in each particular case.

poisoned surfaces might end up being the observed rate-determining step.

For Pd(111), the lowest energy barrier corresponds to the methylinic dehydrogenation, where the activation energy, 0.47 eV, is on the order of the desorption energy, 0.46 eV. The O−H dehydrogenation has a rather high activation barrier of 0.71 eV and it is thus not feasible. These results are in qualitative agreement with reported values.[49] The main pathway is $CH_3OH \rightarrow CH_2OH \rightarrow CHOH \rightarrow COH \rightarrow CO + H_2$, the subsequent activation barriers being 0.45, 0.34, and 0.84 eV, respectively. Because the last step has a relatively high activation energy, the reaction can also follow the alternative path $CHOH \rightarrow CHO \rightarrow CO + H_2$, with activation energies of 0.56 and 0.26 eV. The energy profile shows the largest energy span[50] among the four surfaces and thus it is the worst to decompose methanol. The experimental decomposition to CO and H_2 was experimentally reported to occur around 250 K.[51] The C−O breaking of methanol was found to be not likely, with a high energy barrier of 1.57 eV, in good agreement with a previous theoretical study (not ZPE corrected 1.78 eV).[52]

For Pt we discuss two routes. The loss of the methylenic hydrogen drives the reaction according to the following elementary steps: $CH_3OH \rightarrow CH_2OH \rightarrow CHOH \rightarrow COH \rightarrow CO + H_2$. Once the first barrier (0.65 eV) is overcome, the reaction will proceed to CO with low energy barriers of 0.57, 0.69, and 1.06 eV. Alternatively, the route $CHOH \rightarrow CHO \rightarrow CO + H_2$ has energy barriers of just 0.28 and 0.32 eV. After full dehydrogenation, CO removal is likely to be the bottleneck, as it can accumulate and poison the surface. Our results are in good agreement with experiments, which determined that the methanol dehydrogenation on Pt(111) occurs at temperatures as low as 140 K,[9] significantly lower than the previously reported 250 K Pd value. Yet, another possible route is $CH_3OH \rightarrow CH_3O \rightarrow CH_2O \rightarrow CHO \rightarrow CO + H_2$. In this route, the first reaction is O−H bond scission, which is also the most demanding energy step with an energy barrier of 0.69 eV, followed by moderate barriers of 0.18, 0.28, and 0.32 eV, which facilates the decomposition reactions. According to these results, an isolated methanol molecule will desorb rather than react on Pt(111),[11] and if any reaction takes place, the C−H dehydrogenation would be preferred to the O−H breaking,[8] given that CH_3O is rather unstable on Pt(111), a fact that has been confirmed by experiments.[10] Nevertheless, experimental observations on the dehydrogenation of methanol and other monoalcohols on Pt(111) detected the methoxy radical as an intermediate, but not CH_2OH.[9,53] The source of this apparent discrepancy is that the former analysis does not consider the effect of neighboring methanol molecules, which might play a significant role in O−H bond breaking (see below).

Role of Lateral Interactions. As we have indicated earlier, there are some apparent contradictions between experimental and theoretical results corresponding to the first stage of

DOI: 10.1021/cs501698w
ACS Catal. 2015, 5, 1027−1036

dehydrogenation. Lateral interactions based on hydrogen bonds could be responsible for most of the phenomena regarding O−H groups on metal surfaces.[5,54] Methanol adsorption energy on Cu, Ru, Pd, and Pt is −0.37, −0.59, −0.46, and −0.44 eV, respectively. The hydrogen bond is one of the main lateral interactions between adsorbed methanol molecules, being exothermic by around −0.20 eV. Therefore, under the initial conditions on the clean surfaces, the methanol molecules will approach each other and thus a relatively high coverage even at medium pressures and low temperatures can take place.

In Figure 5 we show that the inclusion of neighboring methanol molecules changes the reaction and activation

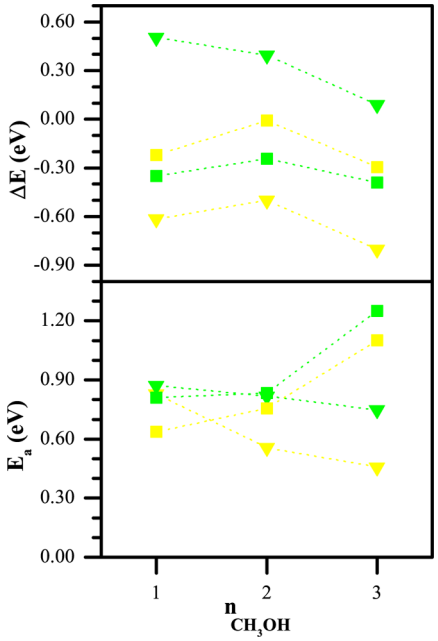

Figure 5. Reaction energies and activation barriers for the dissociation of methanol through the competing O−H (triangles) and C−H (circles) bond breaking, as a function of methanol coverage for Pt(111) (green) and Ru(0001) (yellow).

energies for both O−H and C−H decomposition as follows. On one hand, the nearby OH groups stabilize the methoxy intermediate via hydrogen bonding by around 0.20 eV for each group. They also stabilize the transition state of the O−H decomposition and lower the activation energy by around 0.10−0.20 eV/spectator molecule. On the other hand, the activation barrier for the C−H decomposition increases around 0.10 eV if one spectator methanol molecule is included and then additionally increases by 0.40 eV if a second molecule is incorporated, due to strains in the transition state. The barriers for the competitive reactions at low coverage on Ru favor C−H bond breaking with ΔE_a = 0.19 eV, but at high coverage this value is −0.64 eV, and the values are +0.05 to −0.50 eV for Pt. Therefore, the surrounding methanol molecules will induce a change in the reaction pathway. This is not so clear for Pd, for which the energy difference between both paths is still within the energy change of the lateral hydrogen interactions.

Other intermediates or products can be affected by lateral interactions. For instance, for CO adsorption in dense layers a significant reduction of the average binding energy has been found.[55]

Energy Profiles for the Inverse Reaction: CO Hydrogenation. Over the paths for methanol decomposition, those for synthesis from CO and H_2 without considering the role of CO_2 and/or the water−gas shift reaction can be superimposed to clarify some aspects of methanol synthesis (see Figure 6).

As for the CO hydrogenation, the profiles show that the CHO formation is much more preferable than COH, as the required energies for CHO (COH) formation are 0.17 (2.41) on Cu(111), 0.94 (1.53) on Ru(0001), 1.82 (1.99) on Pd(111), and 1.51 (1.70) eV on Pt(111), respectively. Because of the upright CO adsorption on the four surfaces with C atoms, the interactions between carbon and H atoms are much stronger than those between oxygen and H atoms, which eventually leads to the formation of C−H bonds instead of O−H bonds. For Cu(111) the reaction goes through the adsorption of CO and H_2, forming CHO, which further evolves toward formaldehyde (CH_2O). This formaldehyde preferentially desorbs from the surface. Only if there is a trap for formaldehyde (such as an oxide as in Cu/ZnO[4]) or the amount of H is extremely high could the reaction end up in the formation of methanol. In the modeling of CO_2 electroreduction also some selectivity issues were found on the copper case compatible with our analysis.[56]

The reactions on Ru(0001) are rich, as there are abundant intermediate species and close energy barriers (0.65−0.95 eV) for C−H, C−O, and O−H bond breaking and formation. It should be pointed out here that formaldehyde is the crucial intermediate in the reaction network. The three elementary reactions starting from formaldehyde are $CH_2O \rightarrow CH_3O$, $CH_2O \rightarrow CH_2OH$, and $CH_2O \rightarrow CH_2 + O$. It is interesting to find that they have extremely close barriers of 0.73, 0.70, and 0.72 eV, respectively. Hence, all three reactions can take place in the system. However, the methanol formation from CH_3O is hindered by the largest barrier, 1.34 eV. On the other side, the energy barriers for decomposition from CH_2OH to CHOH (0.21 eV) or CH_2+OH (0.68 eV) are lower than that for methanol formation (0.87 eV). Furthermore, the decomposition from CHOH to CH and OH requires only 0.44 eV and is very exothermic (−1.17 eV). From the above analysis, it is clear to demonstrate that the C−O bond activation reactions are favored on the Ru(0001) surface and, to some extent, methanol formation is unlikely on Ru(0001), as C and O species poison the reactive sites.

On Pd(111), there are two competiting reactions from CHOH: $CHOH \rightarrow CH_2OH$ and $CHOH \rightarrow CO + OH$. The barriers (and reaction energies) are 1.14 (0.69) and 1.18 (−0.06) eV, respectively. Therefore, C−O bond scission from CHOH is most favorable thermodynamically despite similar kinetics. In addition to the CHOH formation, as shown in Figure 6, formaldehyde can also be formed, but it is not as favored as CHOH. There are also two ways for formaldehyde to react on the surface, desorption or hydrogenation to CH_2OH, with energy barriers of 0.75 and 0.90 eV. From CH_2OH, the hydrogenation to methanol is favored, as its energy barrier is 0.95 eV, which is lower than that of C−O bond breaking, 1.31 eV. This reaction barrier is in very good agreement with a previous theoretical study (1.30 eV).[57] Hence, although it seems possible to achieve the methanol synthesis from CO and H_2 on Pd(111), the large barrier for the first hydrogenation step would render the process difficult.

On Pt(111), the first likely intermediate for hydrogenation is CHO followed by CHOH upon the second hydrogenation. Then, the reaction goes as $CHOH \rightarrow CH_2OH \rightarrow CH_3OH$ with activation (reaction) energies of 1.03 (0.46) and 1.16 (0.51) eV. Thus, the network is similar to that of Pd(111); CHOH

DOI: 10.1021/cs501698w
ACS Catal. 2015, 5, 1027−1036

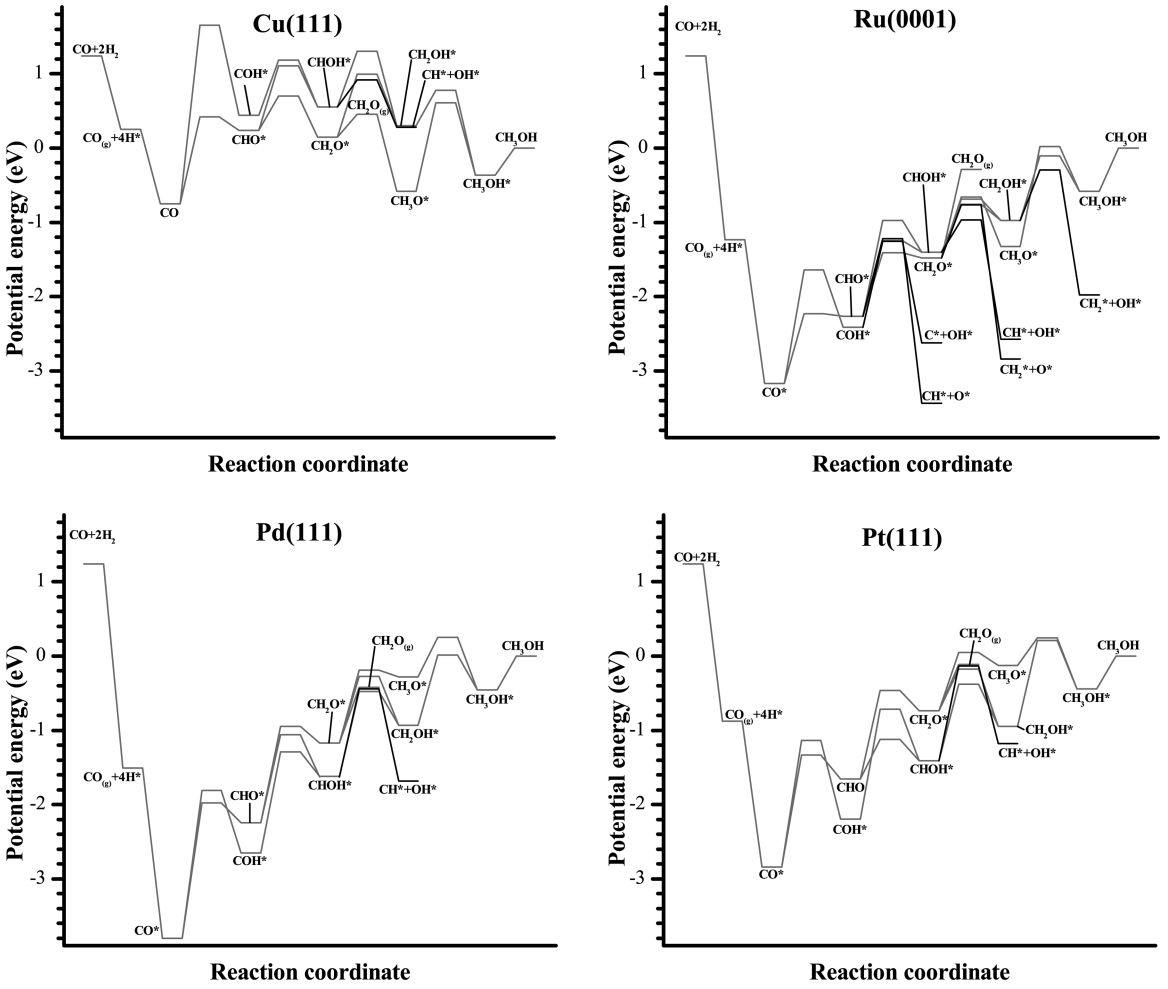

Figure 6. Reaction profiles for the reaction of CO and H_2 on the different surfaces considered here. The minimum energy paths are considered in each particular case.

and CH_2OH are important intermediate species for methanol synthesis. However, it has to be mentioned here that the energy barriers on Pd(111) and Pt(111) are higher than those on other surfaces, and thus these surfaces are less prone to hydrogenate CO.

Kinetic−Thermodynamic Relationships. The relationship between kinetic and thermodynamic parameters was put forward by Brønsted[59] generalized by Evans and Polanyi (BEP),[60] and reintroduced in the density functional theory framework more recently by the groups of Neurock and Nørskov.[61,62] The theory states that the target molecules belonging to a family have similar transition states in nature and thus a change in the thermodynamics of the reaction, i.e. toward more exothermic, is accompanied by a lower activation energy of the direct reaction. If the stability of the intermediates on the surfaces is linked to a single parameter through linear energy scalings,[42] then the BEP relationship directly gives a volcano plot.[63] However, we and others have found that in many cases the BEP relationships represent the dissociation paths better than the associative paths and this behavior has been linked to the early or late-like character of the transition states. An explanation put forward by Hammer[64] indicates that in dissociative paths the interaction between fragments in the transition state resembles that of the final state, provided that this structure corresponds to the fragments sharing some metal atoms in the site ensemble. An alternative formulation of the BEP that allows the systematization for different compounds was presented by Sautet and co-workers.[58,65] These authors employed a general reference and placed the energy of the transition state as a function of either the initial (IS) or the final states (FS). In our case we have employed the two methodologies with the three possible variations (ΔE, IS, FS), to analyze the different classes and deduce the potential relevance of the wide set of data gathered in the present work. The correspoding results are summarized in Figure 7, where all energies contain the ZPE term; to compare only the potential energy values the reader is addressed to Tables S8−S12 and Figures S1−S3 in the Supporting Information.

For the BEP relationships (first column) in Figure 7 it is clear to see that a proper linear dependence is only observed for CH and especially for CO dissociation. In both cases the dispersion is significant in the low energy regime ($\Delta E \leq -1$ eV). In the case of C−H dissociation it seems that the ΔE value is saturated and thus a plateau appears. Indeed, in an understanding of BEP relationships through a Marcus-like approach[66] it becomes clear that for reactions with high endo(exo)thermic energies the values of the activation barrier should be limited by flat areas. The C−H dissociation energies were already reported extensively to show a BEP relationship in the case of the alkyne−alkene−alkane series for a single metal.[18,67] For CO the discrepancy comes from Ru(0001) points that lie at the lowest part of the energy span; in this case the large influence might be

DOI: 10.1021/cs501698w
ACS Catal. 2015, 5, 1027−1036

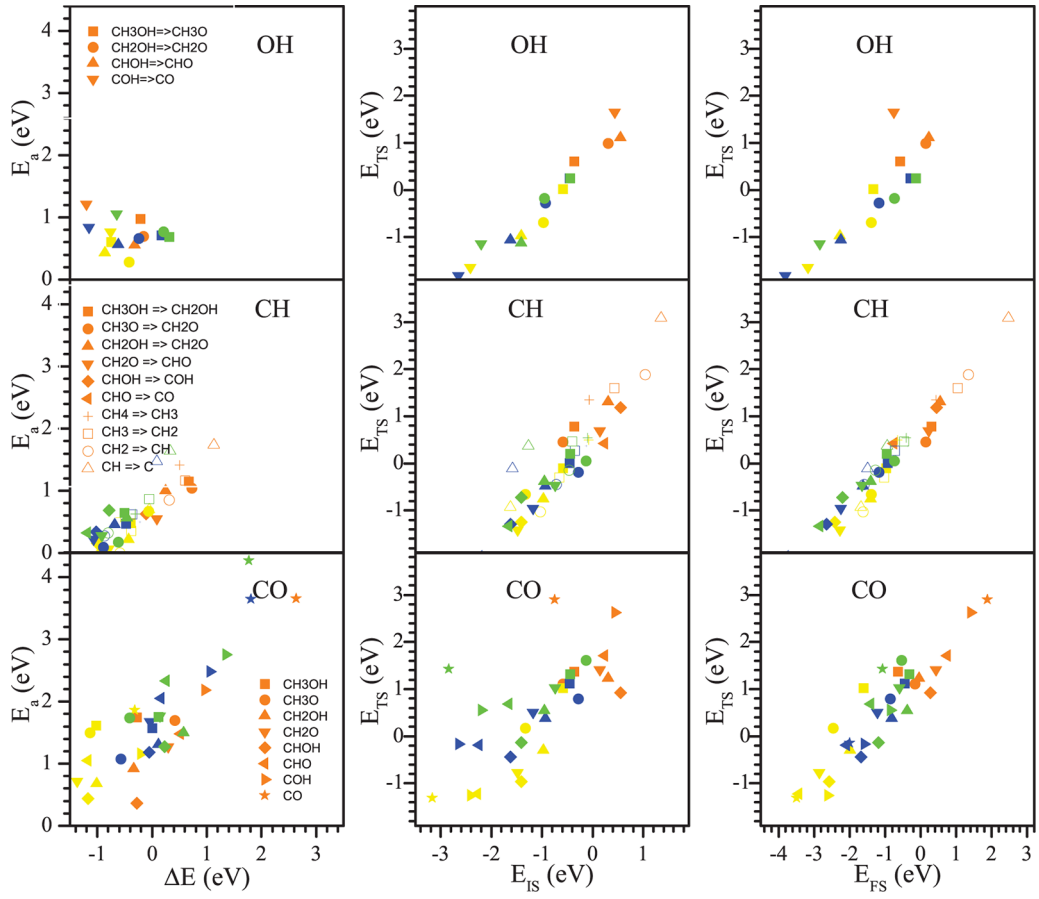

Figure 7. Brønsted–Evans–Polanyi and initial and final state[58] relationships for the different bond breaking reactions: (a) O–H; (b) C–H; (c) C–O. The results of the linear fits are presented in Tables S8–S12 in the Supporting Information.

brought by the strong affinity of Ru toward O atoms (see Table S1 in the Supporting Information).

The situation improves significantly for the dependence on the energy of the initial state, at least for O–H and C–H bond breaking. For O–H a clear line appears with little scattering of around 0.20 eV, the larger being that of Pt (see Figure 7). The values for all metals are distributed quite evenly. The reason for such a good relationship can be traced back to the simple nature of the transition state in this case (Figure 1). A similar, not yet well-defined dependence is found for C–H bonds. In this case the energy span is again large and the points are aligned preferentially on a single line with no semblance of the saturation observed in the BEP plot. However, the point distribution significantly broadens in the central part, where displacements of the individual points to the line can amount up to 0.30 eV. The C–O dissociation class is completely different in this perspective. The list of points is largely scattered, and not even the distribution by individual metals (shown by colors) can illustrate the differences other than from a very qualitative analysis.

Finally, we have considered the dependence of the transition state on the final state energies (third column in Figure 7). For O–H the distribution is no better than that of the initial state. The main reason is the smaller energy span and the appearance of a couple of outliers. When these configurations are analyzed independently, they correspond to Pt and Cu, as in the final state the fragments do not share any metal atoms. In these metals, the FS has no "geometric memory" of the TS, and as described by Hammer[64] the correlation observed for the other points breaks here. For C–H the correlation is excellent and all points show the lowest dispersion from the reference line. The discrepancies are below the 0.20 eV error of DFT, and thus the line can be accepted as presenting an excellent predictive power for this class of reactions. For C–O the final-like transition state nature is nicely captured in the correlation between the transition and final state energies, which gives a good representative character to the BEP line (except for Ru). Since the final states considered here have the fragments sharing same atoms, an even better predicting nature is given to the TS–FS correlation. Discrepancies, for instance the green star at about 0 eV, might be relevant though even on the central part of the point distribution, highlighting that this kind of dissociation, between two heteroatoms that do not differ much in adsorption strength, are the most prone to errors when interpolated.

We note that for several reactions where cooperative, lateral interactions are important, for instance when a web of H bonds is formed, the modification induced by coverage might be much larger than the error made by employing the most suitable kinetic–thermodynamic scaling. Coverage effects in hydroxylic systems might add up an extra 0.15 eV/H bond to the dissociated forms, while the errors of the best prediction curve are around 0.2 eV.

CONCLUSIONS

By means of density functional theory we have investigated the complex networks arising from the decomposition of methanol on four metal surfaces: Cu, Ru, Pd, and Pt. The product

DOI: 10.1021/cs501698w
ACS Catal. 2015, 5, 1027–1036

distributions are different on these metals, where Cu preferentially renders CH_2O, while Pt, Pd, and Ru initially generate large amounts of CO that could potentially poison the surface. The initial decomposition state on Pt and Ru has been a subject of discrepancies between experiments and theory, but coverage effects can fine-tune the relative competing routes. On one hand O−H bond breaking is improved at high coverages while the alternative activation of the methylenic H ends up with an intermediate that requires a larger ensemble and thus is more repulsive. The same set of reactions can be employed to understand the reverse reaction of CO hydrogenation. Again differences in the product distribution appear, Cu being quite unique and the reaction leading to CH_2O. For Pt and Pd the routes to form methanol are affected by CO blocking and the large barriers to transfer the first hydrogen. On Ru, the selectivity problem is more acute, as several routes inducing C−O bond breaking appear at different stages of the hydrogenation. For the kinetic−thermodynamic relationships we have explored different routes to obtain the best-predicting representations. C−H bond breaking is the easiest set of reactions to represent, with almost no error in the TS to FS plot. For O−H the initial state representation seems more adequate, the reason being that the H bond is not as different on the metal surfaces. Activation energies for C−O bond breaking are by far the most difficult to be retrieved. In summary, for complex substrates it would be operative to obtain from the kinetic−thermodynamic scalings the first values for C−H and O−H dissociations and evaluate in detail the more complex C−O dissociations. There is a final point regarding the concept of mechanism in heterogeneous catalysis. According to the IUPAC definition, a mechanism is the list of elementary reactions that lead from reactants to products. However, in line with the complexity of the networks that we observe, the total list of reactions involved might contain a richer information indicating that the set of potential steps is common, although due to the energy differences they are manifested in different "mechanisms".

■ ASSOCIATED CONTENT

Supporting Information

The following file is available free of charge on the ACS Publications website at DOI: 10.1021/cs501698w.

Computed adsorption (with van der Waals contribution analysis), reaction, and activation energies, comparison with previous theoretical and experimental studies, Brønsted−Evans−Polanyi, initial state, and final state scalings, and structures of initial, transition, and final states for all of the reactions in the study (PDF)

■ AUTHOR INFORMATION

Corresponding Author

*N.L.: e-mail, nlopez@iciq.es; tel, +34 977920237; fax, +34 977920231.

Notes

The authors declare no competing financial interest.

■ ACKNOWLEDGMENTS

The authors thank the ERC-2010-STG-258406 Bio2Chem-d project and MINECO (CTQ2012-33826) for financial support and BSC-RES for providing generous computer resources.

■ REFERENCES

(1) Olah, G. A. *Angew. Chem. Int. Ed.* **2005**, *44*, 2636−2639.
(2) Nielsen, M.; Alberico, E.; Baumann, W.; Drexler, H.-J.; Junge, H.; Gladiali, S.; Beller, M. *Nature* **2013**, *495*, 85−89.
(3) Gallagher, J. T.; Kidd, J. M. Patent UK1159035, 1966.
(4) Behrens, M.; Studt, F.; Kasatkin, I.; Kühl, S.; Hävecker, M.; Abild-Pedersen, F.; Zander, S.; Girgsdies, F.; Kurr, P.; Kniep, B.-L.; Tovar, M.; Fischer, R.; Norskov, J.; Schlögl, R. *Science* **2012**, *336*, 893−897.
(5) García-Muelas, R.; López, N. *J. Phys. Chem. C* **2014**, *118*, 17531−17537.
(6) Greeley, J.; Mavrikakis, M. *J. Catal.* **2002**, *208*, 291−300.
(7) Greeley, J.; Mavrikakis, M. *J. Am. Chem. Soc.* **2002**, *124*, 7193−7201.
(8) Greeley, J.; Mavrikakis, M. *J. Am. Chem. Soc.* **2004**, *126*, 3910−3919.
(9) Sexton, B. A. *Surf. Sci.* **1981**, *102*, 271−281.
(10) Karp, E. M.; Silbaugh, T. L.; Crowe, M. C.; Campbell, C. T. *J. Am. Chem. Soc.* **2012**, *134*, 20388−20395.
(11) Desai, S. K.; Neurock, M.; Kourtakis, K. *J. Phys. Chem. B* **2002**, *106*, 2559−2568.
(12) Hammer, B.; Nørskov, J. *Surf. Sci.* **1995**, *343*, 211−220.
(13) Greeley, J.; Nørskov, J. K.; Mavrikakis, M. *Annu. Rev. Phys. Chem.* **2002**, *53*, 319−348.
(14) Nørskov, J. K.; Bligaard, T.; Rossmeisl, J.; Christensen, C. H. *Nat. Chem.* **2009**, *1*, 37−46.
(15) Kang, J.; Nam, S.; Oh, Y.; Choi, H.; Wi, S.; Lee, B.; Hwang, T.; Hong, S.; Park, B. *J. Phys. Chem. Lett.* **2013**, *4*, 2931−2936.
(16) Ferrin, P.; Nilekar, A. U.; Greeley, J.; Mavrikakis, M.; Rossmeisl, J. *Surf. Sci.* **2008**, *602*, 3424−3431.
(17) Yudanov, I.; Matveev, A.; Neyman, K.; Rösch, N. *J. Am. Chem. Soc.* **2008**, *130*, 9342−9352.
(18) Andersin, J.; López, N.; Honkala, K. *J. Phys. Chem. C* **2009**, *113*, 8278−8286.
(19) Wang, S.; Petzold, V.; Tripkovic, V.; Kleis, J.; Howalt, J. G.; Skulason, E.; Fernández, E.; Hvolbæk, B.; Jones, G.; Toftelund, A.; Falsig, H.; Björketun, M.; Studt, F.; Abild-Pedersen, F.; J, R.; Nørskov, J.; Bligaard, T. *Phys. Chem. Chem. Phys.* **2011**, *13*, 20760−20765.
(20) Deckert, A.; Brand, J.; Mak, C.; Koehler, B.; George, S. *J. Chem. Phys.* **1987**, *87*, 1936−1947.
(21) Loveless, B. T.; Buda, C.; Neurock, M.; Iglesia, E. *J. Am. Chem. Soc.* **2013**, *135*, 6107−6121.
(22) Gómez-Díaz, J.; López, N. *J. Phys. Chem. C* **2011**, *115*, 5667−5674.
(23) Kresse, G.; Furthmüller, J. *Comput. Mater. Sci.* **1996**, *6*, 15−50.
(24) Kresse, G.; Furthmüller, J. *Phys. Rev. B* **1996**, *54*, 11169−11186.
(25) Perdew, J. P.; Burke, K.; Ernzerhof, M. *Phys. Rev. Lett.* **1996**, *77*, 3865−3868.
(26) Blöchl, P. E. *Phys. Rev. B* **1994**, *50*, 17953−17979.
(27) Kresse, G.; Joubert, D. *Phys. Rev. B* **1999**, *59*, 1758−1775.
(28) Lide, D. *CRC Handbook of Chemistry and Physics*, 84th ed.; CRC Press: Boca Raton, FL, 2003−2004; pp 12(19−21).
(29) Clendenen, R.; Drickamer, H. *J. Phys. Chem. Solids* **1964**, *25*, 865−868.
(30) King, H.; Manchester, F. *J. Phys. F: Metal Phys.* **1978**, *8*, 15−26.
(31) Arblaster, J. *Platinum Met. Rev.* **1997**, *41*, 12−21.
(32) Monkhorst, H. J.; Pack, J. D. *Phys. Rev. B* **1976**, *13*, 5188−5192.
(33) Makov, G.; Payne, M. C. *Phys. Rev. B* **1995**, *51*, 4014−4022.
(34) Grimme, S. *J. Comput. Chem.* **2006**, *27*, 1787−1799.
(35) Bučko, T.; Hafner, J.; Lebegue, S.; Angyán, J. G. *J. Phys. Chem. A* **2010**, *114*, 11814−11824.
(36) Błoński, P.; López, N. *J. Phys. Chem. C* **2012**, *116*, 15484−15492.
(37) Almora-Barrios, N.; Carchini, G.; Błoński, P.; López, N. *J. Chem. Theory Comput.* **2014**, *10*, 5002−5009.
(38) Henkelman, G.; Jónsson, H. *J. Chem. Phys.* **2000**, *113*, 9978−9985.
(39) Henkelman, G.; Uberuaga, B. P.; Jónsson, H. *J. Chem. Phys.* **2000**, *113*, 9901−9904.

DOI: 10.1021/cs501698w
ACS Catal. 2015, 5, 1027−1036

(40) Heyden, A.; Bell, A. T.; Keil, F. J. *J. Chem. Phys.* **2005**, *123*, 224101(1−14).
(41) Lin, S.; Ma, J.; Zhou, L.; Huang, C.; Xie, D.; Guo, H. *J. Phys. Chem. C* **2012**, *117*, 451−459.
(42) Abild-Pedersen, F.; Greeley, J.; Studt, F.; Rossmeisl, J.; Munter, T.; Moses, P. G.; Skulason, E.; Bligaard, T.; Nørskov, J. K. *Phys. Rev. Lett.* **2007**, *99*, 016105(1-4).
(43) Lim, K. H.; Chen, Z.-X.; Neyman, K. M.; Rösch, N. *J. Phys. Chem. B* **2006**, *110*, 14890−14897.
(44) Zuo, Z.-J.; Wang, L.; Han, P.-D.; Huang, W. *Int. J. Hydrogen Energy* **2014**, *39*, 1664−1679.
(45) Gu, X.-K.; Li, W.-X. *J. Phys. Chem. C* **2010**, *114*, 21539−21547.
(46) Lin, S.; Johnson, R. S.; Smith, G. K.; Xie, D.; Guo, H. *Phys. Chem. Chem. Phys.* **2011**, *13*, 9622−9631.
(47) Gazdzicki, P.; Jakob, P. *J. Phys. Chem. C* **2010**, *114*, 2655−2663.
(48) Chiu, C.-C.; Genest, A.; Rösch, N. *Top. Catal.* **2013**, *56*, 874−884.
(49) Jiang, R.; Guo, W.; Li, M.; Fu, D.; Shan, H. *J. Phys. Chem. C* **2009**, *113*, 4188−4197.
(50) Kozuch, S.; Shaik, S. *Acc. Chem. Res.* **2011**, *44*, 101−110.
(51) Davis, J.; Barteau, M. *Surf. Sci.* **1987**, *187*, 387−406.
(52) Zhang, C.; Hu, P. *J. Chem. Phys.* **2001**, *115*, 7182−7186.
(53) Rendulic, K. D.; Sexton, B. A. *J. Catal.* **1982**, *78*, 126−135.
(54) Revilla-Lopez, G.; Lopez, N. *Phys. Chem. Chem. Phys.* **2014**, *16*, 18933−18940.
(55) Loffreda, D.; Simon, D.; Sautet, P. *Surf. Sci.* **1999**, *425*, 68−80.
(56) Peterson, A. A.; Abild-Pedersen, F.; Studt, F.; Rossmeisl, J.; Nørskov, J. K. *Energy Environ. Sci.* **2010**, *3*, 1311−1315.
(57) Lin, S.; Ma, J.; Ye, X.; Xie, D.; Guo, H. *J. Phys. Chem. C* **2013**, *117*, 14667−14676.
(58) Zaffran, J.; Michel, C.; Auneau, F.; Delbecq, F.; Sautet, P. *ACS Catal.* **2014**, *4*, 464−468.
(59) Brönsted, J. *Chem. Rev.* **1928**, *5*, 231−338.
(60) Evans, M.; Polanyi, M. *Trans. Faraday Soc.* **1938**, *34*, 11−24.
(61) Pallassana, V.; Neurock, M. *J. Catal.* **2000**, *191*, 301−317.
(62) Nørskov, J.; Bligaard, T.; Logadottir, A.; Bahn, S.; Hansen, L. B.; Bollinger, M.; Bengaard, H.; Hammer, B.; Sljivancanin, Z.; Mavrikakis, M.; Xu, S. Y.; Dahl; Jacobsen, C. *J. Catal.* **2002**, *209*, 275−278.
(63) Bligaard, T.; Nørskov, J. K.; Dahl, S.; Matthiesen, J.; Christensen, C. H.; Sehested, J. *J. Catal.* **2004**, *224*, 206−217.
(64) Hammer, B. *Phys. Rev. Lett.* **1999**, *83*, 3681−3684.
(65) Loffreda, D.; Delbecq, F.; Vigné, F.; Sautet, P. *Angew. Chem. Int. Ed.* **2009**, *48*, 8978−8980.
(66) Marcus, R. A. *Angew. Chem. Int. Ed.* **1993**, *32*, 1111−1121.
(67) García-Mota, M.; Bridier, B.; Pérez-Ramírez, J.; López, N. *J. Catal.* **2010**, *273*, 92−102.

DOI: 10.1021/cs501698w
ACS Catal. 2015, 5, 1027−1036